ADVANCED MATERIALS INTERFACES
Open Access
www.advmatinterfaces.de

Antipolyelectrolyte Response of Amphiphilic Sulfobetaine Polymer Coatings

Lisa Schardt, Stefano Da Vela, Alejandro Martínez Guajardo, Maximilian Jaugstetter, Kristina Tschulik, André Laschewsky, and Axel Rosenhahn**

Zwitterionic, amphiphilic polymer coatings are an effective strategy to decrease biofouling. Yet their performance strongly depends on the mechanical properties, the degree of swelling, and the structure of the swollen hydrogels. These properties depend on the zwitterionic groups in the polymers and the properties of the surrounding electrolyte. Therefore, the influence of the ions present and their concentrations on the swelling behavior of amphiphilic zwitterionic copolymers is studied. Coatings of 3-[*N*-2′-(methacryloyloxy)ethyl-*N*,*N*-dimethyl]-ammoniopropane-1-sulfonate (SPE) with increasing amounts of butyl-methacrylate (BMA) are compared to the respective homopolymers PSPE and PBMA. Surface plasmon resonance spectroscopy shows a salt concentration-dependent anti-polyelectrolyte behavior. A variation of the salts revealed that the anions dominated the swelling response, while a change of cations has hardly any effect. Small angle X-ray scattering reveals the morphological changes in the polymer films that accompanied the swelling. With increasing salt concentration, the internal structure changed from compact pores in a gel-like network to elongated cylindrical pores at higher salinities. The understanding gained from the presented multi-technique approach allows to understand the behavior of zwitterionic coatings in saline solutions and helps to tailor the swelling response and mechanical properties for future marine and medical low-fouling applications.

1. Introduction

Zwitterionic polymers such as 3-[N-2′-(methacryloyloxy)ethyl-N,N-dimethyl]-ammoniopropane-1-sulfonate (SPE) have been established as materials for marine and medical anti-fouling coatings that effectively counteract the attachment of several model foulers such as proteins, bacteria, diatoms, and algae.[1–6] The underlying mechanism of fouling inhibition is explained by the combination of charge neutrality and stable hydration of the polymers.[5–9] As a result, the hydrogel coatings are highly swollen and very soft when exposed to aqueous environments.[10–12] Besides the swelling behavior and the degree of hydration, the mechanical properties are decisive for the successful use in technical applications. Despite the high chemical stability of polymethacrylates, zwitterionic sulfobetaine coatings have limited mechanical strength.[11–13] In marine applications, this limited resilience makes the coatings susceptible to incorporating sediment particles which act as nucleation points for the colonization of the surface by fouling organisms.[12] To address this problem, the addition of a limited amount of hydrophobic units into hydrogels has been identified as a possible way to increase the integrity while maintaining the anti-fouling performance.[2,14–18]

The presence of hydrophobic units in amphiphilic coatings and their effect on swelling and water binding seem essential to develop guidelines for a rational design of amphiphilic hydrogel coatings.[19–21] Especially the presence of salts modifies

L. Schardt, A. Rosenhahn
Analytical Chemistry – Biointerfaces
Ruhr University Bochum
44801 Bochum, Germany
E-mail: axel.rosenhahn@rub.de
S. Da Vela
Hochschule Bremerhaven and guest at Alfred Wegener Institute
27568 Bremerhaven, Germany
The ORCID identification number(s) for the author(s) of this article can be found under https://doi.org/10.1002/admi.202400610

DOI: 10.1002/admi.202400610

A. M. Guajardo, A. Laschewsky
Institute of Chemistry
University Potsdam
14476 Potsdam, Germany
E-mail: laschews@uni-potsdam.de
M. Jaugstetter, K. Tschulik
Analytical Chemistry II
Ruhr University Bochum
44801 Bochum, Germany
A. Laschewsky
Fraunhofer Institute of Applied Polymer Research IAP
14476 Potsdam, Germany

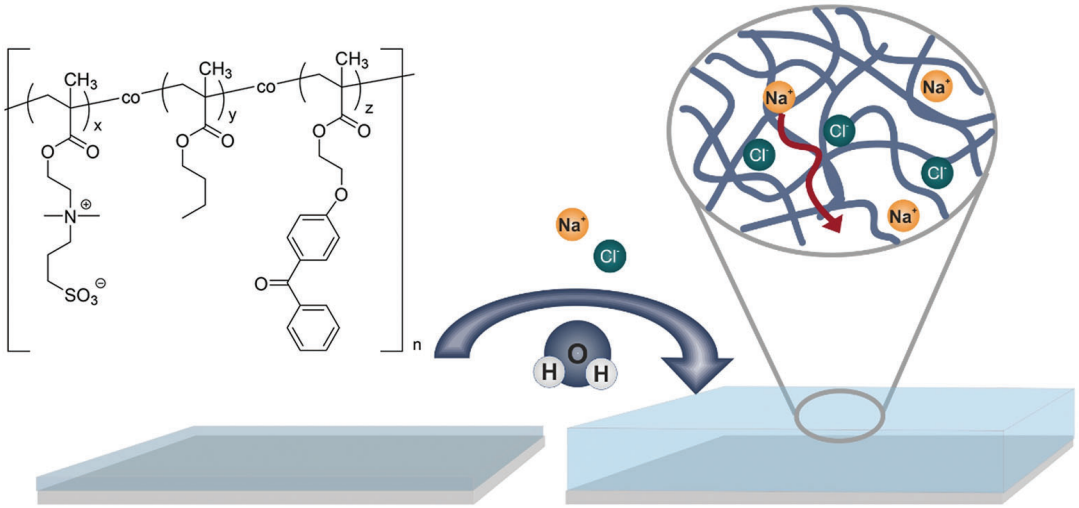

Figure 1. Schematic representation of the SPE-BMA copolymers with different molar fractions x, y and z of the incorporated monomers and the ion induced swelling process.

the solution behavior by affecting the monomer–monomer and monomer–solvent interactions.[22–24] For most zwitterionic polymers, the solubility increases with increasing salinity, so the developed coatings show an anti-polyelectrolyte effect.[23] Inter- and intramolecular Coulombic interactions between the ammonium and sulfonate groups are attenuated due to a Debye-length reduction by the presence of the ions and their competing binding to the ionic groups within the polymer.[24] This leads to a decreased polymer density and diminished interactions within the polymer network in saline solutions compared to purified water.[25,26] Moreover, the polymer chains are often in a collapsed state in purified water, and in a more relaxed one in the presence of salts. As a result, the mechanical properties and the mesh size of the polymer change as well.[27] A relaxational part contributes to the swelling kinetics in addition to the Fickian part describing the diffusion of water into the films.[28,29]

The swelling behavior of SPE-containing hydrogels in saline solutions has previously been studied gravimetrically upon the copolymerization with sodium p-styrenesulfonate,[30] and by SPR upon incorporating hydrophobic moieties containing alkyl side chains.[31] The salt-induced swelling of zwitterionic hydrogels containing SPE[26] and of SPE-based polymer brushes[23,32–35] has been extensively studied in the past. Here, we raise the question how the presence of hydrophobic functional groups influences the swelling and structure of the amphiphilic polymer hydrogels in electrolytes with different salinity (**Figure 1**). To answer this question, we applied in situ picoforce atomic force microscopy (AFM) to gain information about the roughness and film thickness in the dry and swollen states. In addition, surface plasmon resonance spectroscopy (SPR) was utilized for the in situ analysis of the response of the polymer to the presence of different salts across a range of concentrations. As structure sensitive method, small-angle X-ray scattering (SAXS) was used to monitor reorganizations on the nanoscale in the polymer coatings for enhanced structural insight into the anti-polyelectrolyte behavior.

2. Experimental Section

2.1. Sample Preparation

Statistical terpolymers of 3-[*N*-2-(methacryloxy)ethyl-*N*,*N*-dimethyl]-ammoniopropane-1-sulfonate (SPE), *n*-butylmethacrylate (BMA) and 2-(4′-benzoylphenoxy)ethylmethacrylate (BPEMA) were synthesized following previously published protocols.[21] Via free radical copolymerization in solution, different ratios of monomers were combined to synthesize amphiphilic copolymers (**Table 1**). All contain 1 mol% of BPEMA that enables photoinitiated crosslinking. The apparent weight average molar masses M_w of the polymers were between 140 and 490 kg mol^{-1}. Further information about the synthesis and precise ratios of the monomers in the final copolymers can be found in reference.[21]

Gold-coated SPR Chips were functionalized with a monolayer of 11-amino-1-undecanthiol (AUDT, ProChimia) to promote the adhesion of the polymer layer. Following previously published protocols, the substrates were cleaned for 1 h under UV light, rinsed with ethanol (Fisher Scientific), ultrasonicated in ethanol for 3 min, and rinsed with ethanol again before being dried in an N_2 stream. 32.4 mg of AUDT was dissolved in 45 mL of ethanol p.a. before mixing 20 mL of this solution with 38.2 mL of ethanol p.a. and 1.8 mL of triethylamine (≥99.5%, Sigma). The cleaned substrates were immersed in the AUDT solution for 24 h, rinsed with ethanol, ultrasonicated in ethanol for 3 min, rinsed again with ethanol, and dried in a nitrogen stream. The copolymers were dissolved in trifluoroethanol (TFE, >99.8%, Roth) at 0.5 wt.%, and spin-coated (WS-650MZ – 23NPP/Lite, Laurell Technologies Corporation, 15 s at 100 rpm followed by 40 s at 3000 rpm) on the AUDT modified substrates following previously published protocols.[21] The films were cured under UV light (Uvacube 100, Dr. Hönle AG, 100 W iron doped mercury-vapor lamp, H1 filter >310 nm, intensity at sample 15 mW cm^{-2}) for 30 min.

For AFM measurements, silicon wafers (polished, 100, Siegert Wafer) were surface-modified with an aminosilane

Table 1. Polymer composition, sample codes, and captive bubble water contact angles. **PBMA** and **PSPE** are the homopolymers, while coP-* labels precede the copolymers. All polymers contain 1 mol% of BPEMA, for details see ref. [21]

Sample code	Monomer [ratio]		Static water contact angle [°]	Captive bubble contact angle [°]
	SPE	**BMA**		
PBMA	0	100	73 ± 2	42 ± 2
coP-SPE-5-BMA-5	50	50	70 ± 1	14 ± 2
coP-SPE-7-BMA-3	70	30	85 ± 2	13 ± 1
coP-SPE-9-BMA-1	90	10	60 ± 1	10 ± 1
PSPE	100	0	25 ± 3	10 ± 1

adhesion-promoting monolayer underneath the polymer using 3-aminopropyltrimethoxysilane (APTMS, 97%, Sigma–Aldrich) following established protocols.[10,36] The wafers were irradiated with UV light for 1 h prior to immersing them in a solution of 50 mL of acetone (HPLC grade, 99.5+ %, Alfa Aesar) with 2.5 mL of APTMS under nitrogen as inert gas atmosphere for 30 min. Afterwards, the samples were ultrasonicated for 20 s each in ethyl acetate (analytical reagent grade, Fisher Scientific), followed by ethanol and Milli-Q water (Merck Millipore, Darmstadt/Germany). Subsequently, the different polymers were spin coated onto the silanized wafers as described above. To gain absolute values for the layer thickness, measurements were performed at the edge of a scratch made in the middle of the polymer coating.

2.2. Atomic Force Microscopy

A Bruker BioScope Resolve AFM was used in PeakForce Tapping mode at 2 kHz resonance frequency for dry and liquid measurements. For dry measurements a Scanasyst air tip was used, while PeakForce setpoint, amplitude, and scan speed were set to 1.4 nN, 150 nm, and 0.6 Hz, respectively. For liquid AFM measurements the samples were immersed in Milli-Q water for an average duration of 2 h. A Scansasyst fluid tip with a tip diameter of 20 nm was used in liquid. Scan speeds were varied from 0.4 to 1.2 Hz, depending on the scan size to maintain a lateral tip velocity of 4 μms^{-1}. To achieve measurements of the accurate height of the swollen hydrogel PeakForce setpoint and amplitude were slowly decreased from an initial 1.1 nN and 130 nm until the tip lost contact. Measurements were contacted at the minimum force necessary to maintain contact, typical values were 0.4 nN and 90 nm.

2.3. Surface Plasmon Resonance Spectroscopy

An SRC7000DC equipped with a SR7500 pump and SR7100 autosampler (Reichert) was used for the SPR measurements. Milli-Q water was injected at a flow rate of 200 $\mu L\ min^{-1}$ until a stable baseline was obtained, then the flow rate was reduced to 10 $\mu L\ min^{-1}$ for at least 5 min before the injection of the first sample solution. Different salt concentrations were injected for 5 min at a flow rate of 10 $\mu L\ min^{-1}$ before continuing with a higher concentration. Different salt solutions with a constant concentration of 150 mM were injected for 5 or 10 min, followed by a 5/10 min injection of Milli-Q water before the next sample solution, to avoid mixing different ions.

2.4. Small Angle X-Ray Scattering

1 wt.% of copolymers in TFE were filled in quartz capillaries (quartz glass, external diameter 1.5 mm, wall thickness 0.01 mm, Hilgenberg) up to a height of 2 cm. UV light was used to crosslink the polymer for 30 min before the solvent was evaporated in a drying oven for over 48 h and the polymer again exposed to UV light for 30 min. Dry samples were measured as prepared, while for measurements in Milli-Q water or NaCl solution, the solvent was added to the capillary 15 min before the measurement. Capillaries from the same batch filled with air, Milli-Q water, or NaCl solution were used for background subtraction. The subtracted scattering intensity is then the contribution of the polymer layer at the walls of the capillary. It was noted that a similar strategy has been employed in studies which characterized nanocrystal superlattices assembled on silicon nitride windows of a sample cell.[37]

SAXS measurements were performed at the EMBL BioSAXS beamline P12[38] at the Petra III storage ring of the DESY synchrotron radiation source (Hamburg, Germany). The capillaries were measured in a temperature-controlled sample holder using the *in-air* configuration of the beamline (air gap delimited by Kapton windows). For the measurements an X-ray energy of 10 keV and a sample-detector distance of 3.1 m were employed, collecting the scattered radiation with a Pilatus 6 M detector. Angular calibration was performed using the scattering from silver behenate. The resulting accessible range of the momentum transfer q, here defined as $q = \frac{4\pi sin\theta}{\lambda}$ with 2θ being the scattering angle, was 0.03 nm^{-1} < q < 7.2 nm^{-1}. For each measurement, 20 × 35 ms or 45 ms exposures were collected, the corresponding 2D SAXS pattern azimuthally averaged, and the 1D SAXS profiles of the individual exposures averaged after omitting data with noticeable radiation damage. The data reduction was automatically performed by the program SASFLOW,[39] the programs PRIMUS and the ATSAS suite[40,41] were used for initial data processing. Pair-distance distribution functions p(r) were evaluated from the averaged and subtracted intensities I(q) using the program GNOM,[42] and model fitting was performed using SasView.[43]

The overall radius of gyration (R_g) was first extracted without referring to any specific model employing the Guinier approximation for scattering from discrete structural features,[44–46]

which assumes an exponential decay of the scattering intensity as a function of the square of the momentum transfer. The approximation was valid for $qR_g<1.3$ and allows to evaluate R_g from the slope of plots of ln(I(q)) versus q^2 fitted with the equation:

$$ln\,(I\,(q)) = ln\,(I\,(0)) - \frac{1}{3}{R_g}^2 q^2 \quad (1)$$

where I(q) is the measured scattering intensity and I(0) the extrapolated forward scattering. This yields an apparent radius of gyration whose absolute value may be influenced by the surrounding polymer matrix but can still capture the changes in overall size within experimental SAXS resolution manifested in the scattering curves.

For particularly elongated ("rod-like") structures, a similar radius of gyration referring to their cross-section can be extracted.[45] In that case, the equation above is modified and reads:

$$ln\,(q \cdot I\,(q)) = ln\left(I(0)_C\right) - \frac{1}{2}{R_{gC}}^2 q^2 \quad (2)$$

where $I(0)_c$ is the cross-sectional I(0), and R_{gC} is the cross-sectional radius of gyration.

Real-space pair-distance distribution functions P(r), likewise not referring to a specific structural model, can be calculated for the overall structure and the cross-section of elongated structures by indirect Fourier transformation[45,46] of I(q) and qI(q), respectively. Additionally, the Kratky representation of the data $q^2I(q)$ versus q was used to highlight the presence of compact structural features. The I_0 used for the normalization of the Kratky plots was obtained from the PDDF (p(r)) analysis. Linear Guinier regimes at low angles can be interpreted as the overall size of discrete particle-like scatterers falling within SAXS resolution, while the appearance of a linear regime of $ln(q \cdot I(q))$ versus q^2, for $q{\cdot}R_{gC}<1.3$, was suggestive of rod-like structures.[44–46]

The Guinier-Porod model[47] was used to fit the Porod exponent and the R_g of the structures, to gain further insight into the features of the polymer. In this model, R_g and the Porod exponent can be extracted in a shape-independent way for both globular and elongated structures from a fit of the whole curve, with the fit parameter *s* being 0 for spherical objects and 1 for cylindrical objects. The small-angle scattering from gel-like networks was modelled considering two additive contributions, one from the mesh resulting from the gel cross-linking that takes an exponential form, the other one from the fluctuations of the chains (Gauss-Lorentz-Gel).[48] For the latter model the scattering intensity is:

$$I\,(q) = I_G\,(0)\,e^{-\frac{q^2\Xi^2}{2}} + \frac{I_L\,(0)}{(1+q^2\xi^2)} \quad (3)$$

where Ξ is the mesh (static) correlation length, while ξ is the chain (dynamic) correlation length, and $I_G(0)$ and $I_L(0)$ are scaling prefactors. In the Sasview implementation, an overall scaling factor and a background term were added.

2.5. Statistical Analysis

In the AFM measurements, the height was determined at three different positions and averages were reported along with the standard error. For the SPR data, coatings were automatically analyzed in different electrolyte concentrations using autosampler injection. From the fit of the entire dataset using a mixed linear and logistic function, error bars were calculated as the standard error via variance-covariance analysis. For the SAXS curves, MilliQ water or the used NaCl solution at a given concentration in a clean capillary were used for background subtraction. During measurements 20 frames were acquired and each frame was compared and only frames which past similarity test were used for summation. Error calculations were based on Poisson distribution of measured counts.

3. Results and Discussion

Amphiphilic copolymers containing varying ratios of hydrophilic, zwitterionic N-(2-methacryloyloxy) **e**thyl-N,N-dimethylammonio propanesulfonate (SPE) to hydrophobic butyl methacrylate (BMA) and a fixed amount of the crosslinker benzoylphenoxyethylmethacrylate (BPEMA) were synthesized (Table 1). Detailed information about the synthesis and analytical data was published previously.[21] Copolymers with > 50 mol% BMA were not considered as they were no more water soluble and thus found to be unsuited for the presented hydration study. The contact angle in air of the resulting polymer films varied between 73 ± 2° for poly(butylmethacrylate) (**PBMA**), and 25 ± 3° for the poly(sulfobetainemethacrylate) (**PSPE**). Upon immersion in saltwater, the captive bubble contact angles changed to 42 ± 2° for **PBMA** after 7 days, and to 10 ± 1° for **PSPE**. The most drastic reduction in contact angle was observed for the amphiphilic copolymers. Due to a strong surface rearrangement, the contact angles decreased from 60° to 70° resulting in underwater contact angles of 14° ± 2° for **coP-SPE-5-BMA-5**, 13° ± 1° for **coP-SPE-7-BMA-3**, and 10° ± 1° for **coP-SPE-9-BMA-1** (Table 1).

3.1. In Situ Analysis of the Response of the Polymers to Different Electrolyte Concentrations Studied by SPR

SPR detects changes in the optical density at the liquid-solid interface between the chip and the solution in the flow channel. Monitoring the response of the polymer to different, subsequently injected solutions in real time, provides quantitative details on the polymer response as well as kinetic information. The method was used to study the anti-polyelectrolyte response of the zwitterionic hydrogel coatings in contact with different salt solutions. With a polymer thickness of ≈50 nm, the coatings are inside the penetration depth of the evanescent field both in the collapsed and in the fully swollen states (**Figure 2**).

The sensograms in Figure 2 show the response of the SPR signal when NaCl solutions with increasing concentrations from 0.29 to 1000 mM were injected using an autosampler with a close-up of a single injection phase in Figure 2C. The injection phases are marked by the gray background, while in sections with white background, the flow was switched back to Milli-Q water. The

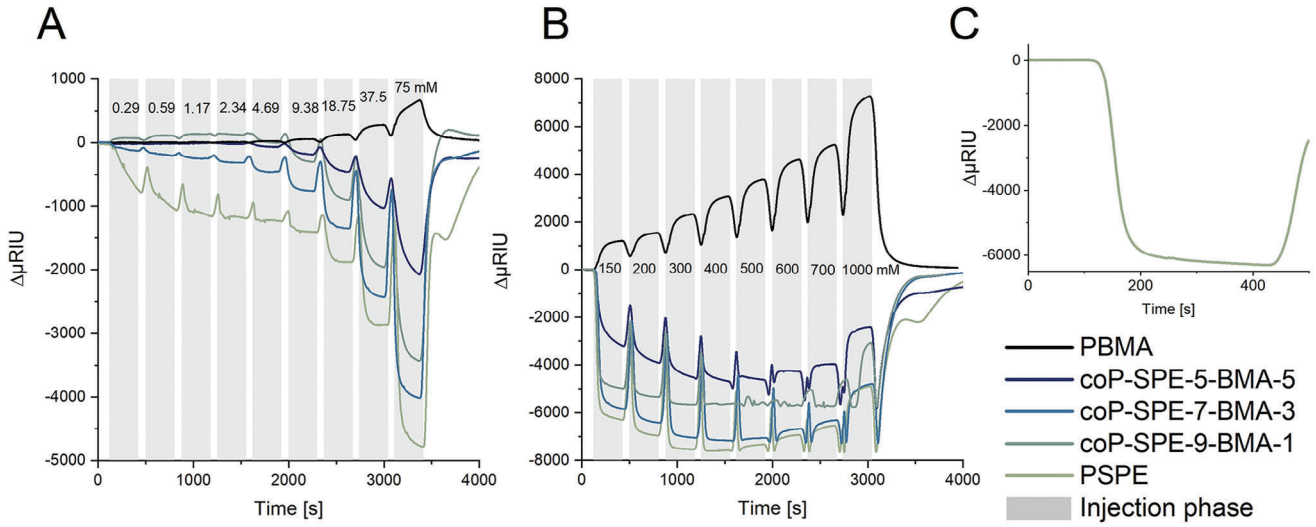

Figure 2. SPR sensorgrams of amphiphilic BMA/SPE copolymers for low NaCl concentrations between 0.29 and 75 mM A), and high NaCl concentrations between 150 and 1000 mM B). A single injection phase (**PSPE**, 150 mM) is shown enlarged in C).

hydrophobic **PBMA** coatings showed in general a low swelling and just a slight reorientation as apparent in the contact angle change. Upon a change in salinity, we do not expect any changes as the increased salinity is unlikely to interfere with the van-der Waals interactions between the BMA moieties. Consequently, the SPR response during the injection phases of the different NaCl concentrations increased as the refractive index of the solution increased. During the Milli-Q phases, the response decreased again as the optical density of the solution decreased. At the end of the experiment, the flow was switched back to Milli-Q water (Figure 2B) and the SPR signal returned to the initial value, indicating that the SPR response was reversible. **Figure** 3A shows that the SPR signal increased linearly with the salt concentration. A comparison with the response of an uncoated gold chip shows that the response on the **PBMA** coated samples was only 65% ± 1% of the response of the uncoated chip (Figure 3A). The reduced response of the **PBMA** coatings has been caused by the exclusion volume above the gold films occupied by the **PBMA** which was not accessible for the electrolyte solution. Thus, only the part of the evanescent field that extended above the **PBMA** film detected a change in refractive index, leading to the lower response compared to the bare gold SPR chip.

In contrast to the hydrophobic **PBMA**, the zwitterionic **PSPE**s responded by a negative shift of the surface plasmon resonance (Figure 3B). Up to a NaCl concentration of 400 mM, the negative shift increased, while above 400 mM, the SPR signal shifted to larger values. This indicates that two different processes caused the plasmon resonance response. The decrease of the signal at low salt concentrations can be explained by the anti-polyelectrolyte behavior of the zwitterionic coatings, namely the salting-in effect, which results in a swelling of the films by increased water uptake. The swelling leads to a less dense polymer (lower refractive index) with a higher thickness, i.e., the same amount of polymer is "stretched" over a larger volume. The total amount of polymer during this process remains the same and stays entirely within the evanescent field, as revealed by the AFM

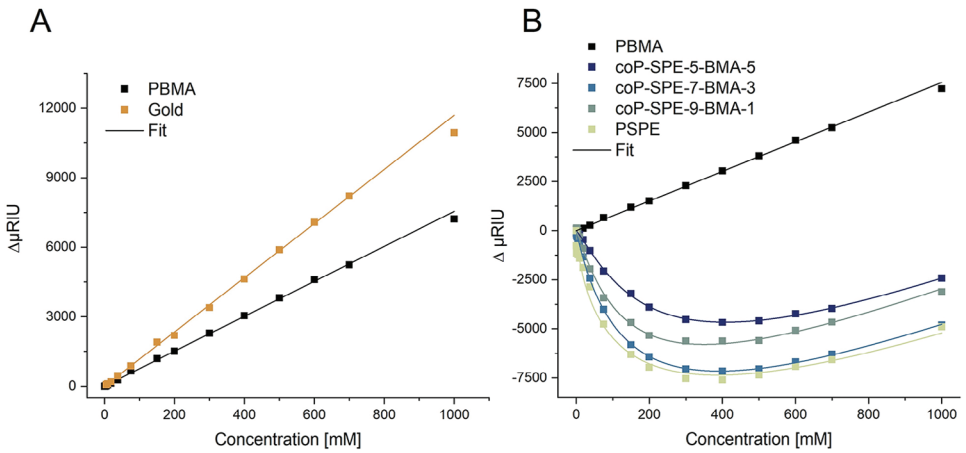

Figure 3. A) SPR signal change for gold and **PBMA** in the presence of electrolytes with different NaCl concentrations. The straight lines reflect linear fits. B) Fit of the shift in the SPR signal relative to Milli-Q water for 0.29–1000 mM NaCl solutions.

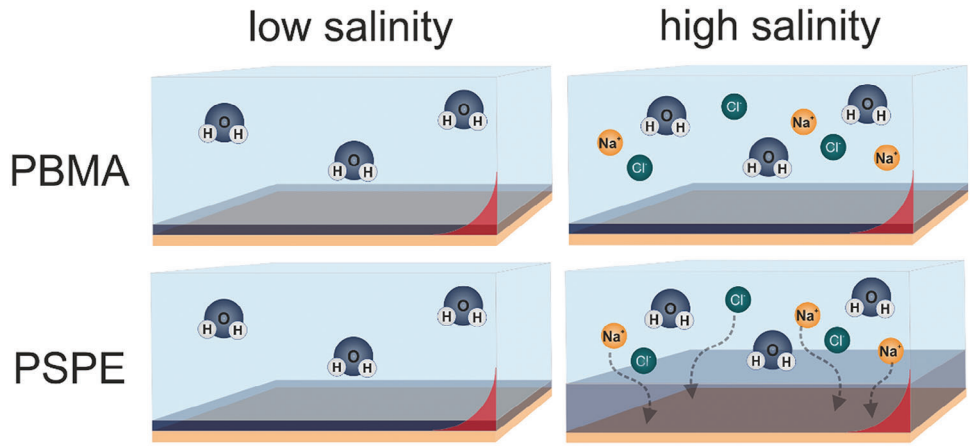

Figure 4. Schematic illustration of the swelling of **PBMA** and **PSPE** films in low and high salinity solutions. The red area illustrates the decay of the evanescent field.

thickness measurements discussed below. This redistribution of a dense polymer close to the gold layer into a less dense, thicker layer lead to a redistribution of the organic material within the exponentially decaying evanescent field (**Figure 4**). The amount of polymer sensed by the stronger part of the evanescent field close to the surface is reduced, which leads to the observed reduction of the SPR signal. While the redistributed fraction of the polymer is still sensed, the evanescent field in this region is already decayed and thus the SPR response is weaker and not able to fully compensate the signal reduction close to the gold surface. The processes occurring on the non-swelling **PBMA** coatings and on the **PSPE** coatings with anti-polyelectrolyte behavior are schematically depicted in Figure 4. This polymer swelling overcompensated the refractive index increase caused by the increased salt concentration. At ≈ 400 mM NaCl concentration, the anti-polyelectrolyte effect became weaker as most electrostatic interactions were screened and the polymer chains had fully extended. From this point on, the increasing refractive index due to the increased salt concentration dominates the SPR response and the signal starts to increase.

When comparing the anti-polyelectrolyte responses in the sensorgrams for the different amphiphilic polymers (Figure 3B), the pure **PSPE** films showed the strongest anti-polyelectrolyte effect. The amphiphilic copolymers showed a similar behavior as **PSPE**, but the overall shifts of the plasmon resonance were lower. This reflects the lower swelling of the BMA-containing copolymers. The very similar shape of the curves at high salinities was caused by the refractive index of the NaCl solution. Comparing the three co-polymers, **coP-SPE-5-BMA-5** had the lowest signal shift, as was expected due to the lowest content of polymer-attached ionic groups. **coP-SPE-7-BMA-3** showed a more negative signal shift than **coP-SPE-9-BMA-1**. This counter-intuitive SPR response did not follow the observed trend of increasing swelling with increasing SPE content. Nonetheless, the overall reduced swelling of the BMA containing copolymers compared to the pure **PSPE** suggests that the attractive van-der-Waals interactions between the hydrophobic BMA side chains limited the swelling, and thus restricted the expansion of the polymer coating.

A phenomenological model of the polymer response to different salinities was developed to extract characteristic numbers like the slope or the minimum of the curves. First, the contribution of the optical density of the different salt solutions was fitted. For the blank gold chip, a linear function with a slope of a = 11.7 ± 0.3 µRIU/mM (R^2 = 0.998) described the observed changes best. The smaller magnitude of the accessible evanescent field in the **PBMA** measurements was reflected by the reduced slope of 7.39 ± 0.1 µRIU/mM (R^2 = 0.999). By dividing the signal shift for gold by the signal shift of **PBMA** resulted in a relative difference c = 0.645 ± 0.005. It was possible to model the SPR response at different salinities by a combination of a linear function to account for the salinity change and a logistic function that describes the swelling behavior as a function of salinity (Equation 6):

$$y = a \cdot c \cdot x - \left(A_2 + \frac{A_1 - A_2}{1 + \left(\frac{x}{x_0}\right)^p} \right) \quad (6)$$

with A_1 being the minimum swelling, which is set to 0 in Milli-Q at the beginning of the experiment. A_2 represents the maximum swelling capacity, x_0 is the position of the inflection point, and p determines the steepness of the logistic contribution.

The developed model was applied to the experimental data (Figure 3B, solid lines), and the obtained fitting parameters are given in **Table 2**. The correlation between the measured data and the fitted curves was very high, as indicated by R^2 = 0.98 for **PSPE** and R^2 >0.99 for all other polymers. The maximum possible swelling A_2 tended to increase with the increase in SPE content from **coP-SPE-5-BMA-5** over **coP-SPE-9-BMA-1** to **PSPE**.

Table 2. Fit parameters of the SPR response curves according to Equation (1) for the used NaCl concentration range between 0.3 and 1000 mM. Errors are the standard errors obtained via variance-covariance analysis.

	A_2 [µRIU]	x_0 [mM]	P [-]	R^2
coP-SPE-5-BMA-5	11882 ± 133	235 ± 6	1.14 ± 0.02	0.9994
coP-SPE-7-BMA-3	14416 ± 178	163 ± 5	0.98 ± 0.02	0.9993
coP-SPE-9-BMA-1	11893 ± 294	153 ± 10	1.08 ± 0.05	0.9961
PSPE	16853 ± 1757	209 ± 70	0.73 ± 0.08	0.9758

Yet, **coP-SPE-7-BMA-3** had the highest A_2 of all copolymers, falling still short of homopolymer **PSPE**. The strongest concentration dependence of the swelling, reflected by the position of x_0, was reached in a relatively narrow concentration range between 150 and 250 mM NaCl and the differences exceeded the error bars only for **coP-SPE-5-BMA-5**. Within the amphiphilic copolymers from **coP-SPE-5-BMA-5** to **coP-SPE-9-BMA-1**, one might note a shift of x_0 to lower concentrations with increasing SPE content.

The last parameter is the exponential factor p which reflects the steepness of the logistic contribution and accounts for the shape of the swelling curve particularly in areas with a negative slope (Figure 3B). High values of p can be interpreted as a completion of the screening of the attractive electrostatic interactions within the zwitterionic polymer in a relatively small salt concentration range. Thus, high values of p indicate that the interactions were screened between different side chains and thus, their chemical natures were highly similar. Otherwise, the attractive interactions would not be lifted at approximately the same concentration. In contrast, low p values correspond to a slower increase of the swelling curve with increasing salt concentrations caused by interactions breaking in a broader concentration range. Thus, the attractive interactions between the polymer chains, e.g., the chemical nature and the number of chemical groups involved, are more diverse. As shown in Table 2, the fitted p values are higher for all mixed copolymers than for **PSPE**, indicating that the attractive interactions in the latter polymer are chemically more similar than in the copolymers.

SPR measurements show that the polymer networks reach their full extension at NaCl concentrations ≈200–500 mM. The observation that all polymers respond at a very similar electrolyte concentration range indicates similar interactions between the zwitterionic groups. Above 500 mM, most attractive electrostatic interactions are quenched, while the crosslinking of the polymer prevents further swelling at even higher salt concentrations. With increasing ion concentration, the refractive indexes of the solution and the hydrated polymer further increase, leading to a positive slope of the SPR response curve. At very low salt concentrations, ion diffusion is controlled by the concentration gradient between solution and polymer coatings, with the zwitterionic groups of the polymer contributing to the osmotic gradient.[24] The zwitterionic groups have a specific ionic strength that forms an osmotic barrier counteracting the diffusion into the polymer if the ionic strength of the polymer is higher than the ionic strength of the electrolyte.[24] Nearly no swelling was detected at low salt concentrations between 0.2 and 2.3 mM NaCl for polymers rich in zwitterionic groups, which was particularly the case for **coP-SPE-9-BMA-1** and also observed in **PSPE**. While these influences on the swelling in the low and high salt regimes are relatively well understood, interpreting the intermediate region is more challenging. Both, the salt concentration, which promotes solubility of the polymer chains, and the restriction of the vertical extension of the polymer network due to the crosslinks determine the equilibrium state of the polymer.

The attractive electrostatic interactions between the oppositely charged groups in the zwitterionic polymer could either occur as 1:1 with two side chains placed in opposite directions or with three or more side chains forming more complex geometries.[49,50] The variety and complexity of these interactions are reflected in the fit parameter p in Equation (6). If the type of interaction between adjacent polymer chains is highly uniform, e.g., always electrostatic attraction between two oppositely charged groups of the zwitterion, they are expected to be broken in a narrow concentration range. Hence, larger values of p are expected. However, if the side chains of the polymer interact by several different interactions in different geometries, the interactions will break at different salinities. This results in a more stretched swelling curve and, thus, in smaller values of p. The comparison between **PSPE** and the amphiphilic copolymers showed that **PSPE** had an exponent p of 0.73 ± 0.08, which was lower compared to the copolymers with 1.08 ± 0.05 for **coP-SPE-5-BMA-5**, 0.98 ± 0.02 for **coP-SPE-7BMA-3**, and 1.14 ± 0.02 for **coP-SPE-5-BMA-5**. The introduction of additional chemically different side chains increased the number of possible interactions and interaction geometries between polymer chains within the copolymer. Due to the difference in polarity, BMA and SPE did not interact strongly enough with each other to inhibit the swelling of the polymer and rather form purely hydrophilic or hydrophobic interactions. On top of that, BMA separates SPE side chains from each other, resulting in fewer possible geometries for attractive electrostatic interactions between the oppositely charged groups of the zwitterionic moieties.

In both physiological and marine environments, not only NaCl but also other mono- and multivalent ions are present. To understand the interaction of the different zwitterionic polymers with different cations and anions, the SPR response to various monovalent salts at a constant concentration of 150 mM has been investigated. At this concentration, the polymer is not entirely swollen, and the obtained SPR shifts reflect how strongly the anti-polyelectrolyte effect is induced by the different ions of increasing chaotropic character, meaning they have an increasingly lower surface charge density.[51] To avoid mixing different salts in the polymer, each injection of a saline solution was followed by a Milli-Q water injection phase to remove as much salt as possible. **Figure 5** shows separated peaks upon the injection of a saline solution which returned reasonably close to the Milli-Q water baseline after the salt injection finished. In agreement with the NaCl measurements, the SPR shifts were positive for the gold reference and **PBMA**. However, for **PSPE** and the copolymers, the signal was negative upon salt injection, indicating a relatively strong swelling of the polymers. This reduced the optical density of the polymer close to the chip surface and overcompensated the increase in the optical density of the electrolyte solution, for the reasons discussed above. An increasingly negative signal was detected for films from **coP-SPE-5-BMA-5** over **coP-SPE-7-BMA-3** and **coP-SPE-9-BMA-1** to **PSPE** when exposed to solutions containing NH_4Cl, i.e., the salt made of anion and cation with the least chaotropic characters within the Hofmeister series amidst the investigated salts.[52,53] However, this trend changed for **coP-SPE-7-BMA-3**, which had a comparable shift to **coP-SPE-9-BMA-1** in solutions containing KBr and the various nitrate salts. In the iodide-containing solutions, **coP-SPE-7-BMA-3** even showed an intermediate response between **coP-SPE-9-BMA-1** and **PSPE**.

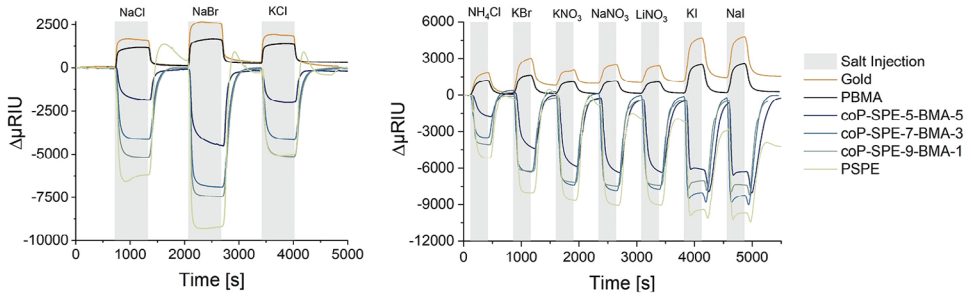

Figure 5. SPR curves of amphiphilic BMA/SPE copolymers films swollen in 150 mM solutions of different monovalent salts.

The magnitude of signal change was different for the different electrolytes. The response increased in the order $Cl^- < Br^- < NO_3^- < I^-$, following their increasing chaotropic character, while the cations only showed negligible effects on the SPR response. In most cases, the swelling of the polymers dominated the individual peak shapes with a fast decrease upon injection of the saline solution and an additional slower decrease until the swelling reached its equilibrium state. For iodine-containing salts, the swelling was close to the maximum swelling capacity of the polymer given by the crosslinker content. The signal decreased quickly at the beginning of the injection until the maximum swelling capacity of the polymer was reached. Beyond this point, there was a further diffusion of salt solution of a high optical density into the polymer, but no more swelling. As a result, the signal rised again. Upon the end of the iodide-containing salt injection, the reversal of this process was observed. The saline solution diffused out of the polymer upon the start of the injection of Milli-Q while the polymer was still at its maximum swelling, resulting in an increasingly negative SPR signal. After a few seconds, the salt concentration was low enough for the polymer to start to shrink, and the signal rose again.

To decouple the response of the polymer from the influence of the saline solutions, the gold reference was subtracted from the polymer curves. A negative response caused by the swelling was measured for all polymers. The maximum of the resulting signal intensities for the different anion/cation combinations was determined and plotted as a heat map (**Figure 6**). The **PBMA** signal change was about one order of magnitude smaller, even for the I^- containing salts, which promoted the strongest swelling response of the polymer. The hydrophobic nature of **PBMA** and its corresponding weak swelling creates a volume above the gold layer inaccessible to the electrolyte, which reduces the SPR response to changes in refractive index of the electrolyte compared to the uncoated gold chip. The swelling of the SPE-containing polymers caused strong SPR shifts toward lower optical densities due to the swelling of the polymers and the resulting redistribution of the polymer within the evanescent field. The plots in Figure 6 show that for all polymers with zwitterionic content, the anions had the strongest influence on the swelling response of the polymers, while the variation of the cations in the range of studied electrolytes, had only minor effects on the swelling. This is in good agreement with several studies reporting that the swelling of zwitterionic polymers in salt solutions depends mostly on the nature of the anion.[23,28,50] Within the series of anions, the swelling increases corresponding to the Hofmeister series.[50,54]

3.2. Swelling of the Coatings Analyzed by AFM

To gain additional information about the surface structure and the absolute height of the polymer films, AFM was measured in air and in water (**Figure 7**). A wide scratch, visible as the lower part on the right side of the images, was cut into the coatings down to the substrate to determine the height. Note that conventionally AFM is typically operated at setpoints of more than 10 nN, which is well suited to analyze the height of the dry polymers at the edges of the scratches with high accuracy. In the hydrated state, however, highly swollen polymers, such as the studied zwitterionic coatings, become hardly measurable with liquid AFMs operating at such conventional setpoints, as the tip penetrates through the hydrated and soft hydrogel. Thus, the images only show the hard substrate. We therefore utilized the PeakForce Tapping mode of a Bruker Bioscope AFM, a very low setpoint of down to 200 pN, and a blunt probe of 20 nm tip radius. This measurement procedure minimizes material uptake and immersion into the low-density layers, by decreasing both pressure and dwell time during hydrogel-tip contact.

Using this setup, an analysis of the film thickness and the surface morphology of the swollen and hydrated films was possible. The measurements revealed that the dry polymer coatings have an average thickness of 113 ± 10 nm independent of the chemical nature of the polymer (**Figure 8**). All surfaces were characterized by a smooth appearance within the given resolution (Figure 7). When measuring in water, the polymers layer thicknesses increased significantly with notable differences among the different chemical composition. The thickness of the **PBMA** films increased by only 17% while **PSPE** increased by 119% (Figure 8). **coP-SPE-9-BMA-1** showed an increase in layer thickness of 129%. **PSPE**, **coP-SPE-7-BMA-3** and **coP-SPE-5-BMA-5** behaved very similarly with an increase in layer thickness under water of 75% and 82%, respectively. The swelling of these copolymers with intermediate SPE contents had a magnitude between **PSPE** and **PBMA**. Thus, all copolymers showed substantial swelling in water, despite the presence of the hydrophobic BMA building blocks. The high swelling capacity of the amphiphilic copolymers caused roughly a doubling of the coating thickness in water for all SPE containing polymers, with a tendency toward stronger swelling for coatings with a higher SPE content. Copolymers **coP-SPE-5-BMA-5** and **coP-SPE-7-BMA-3** exhibited a uniform and smooth surface texture, while **coP-SPE-9-BMA-1** showed a slightly rougher surface with a noticeable granular structure in the dry and the wet state.

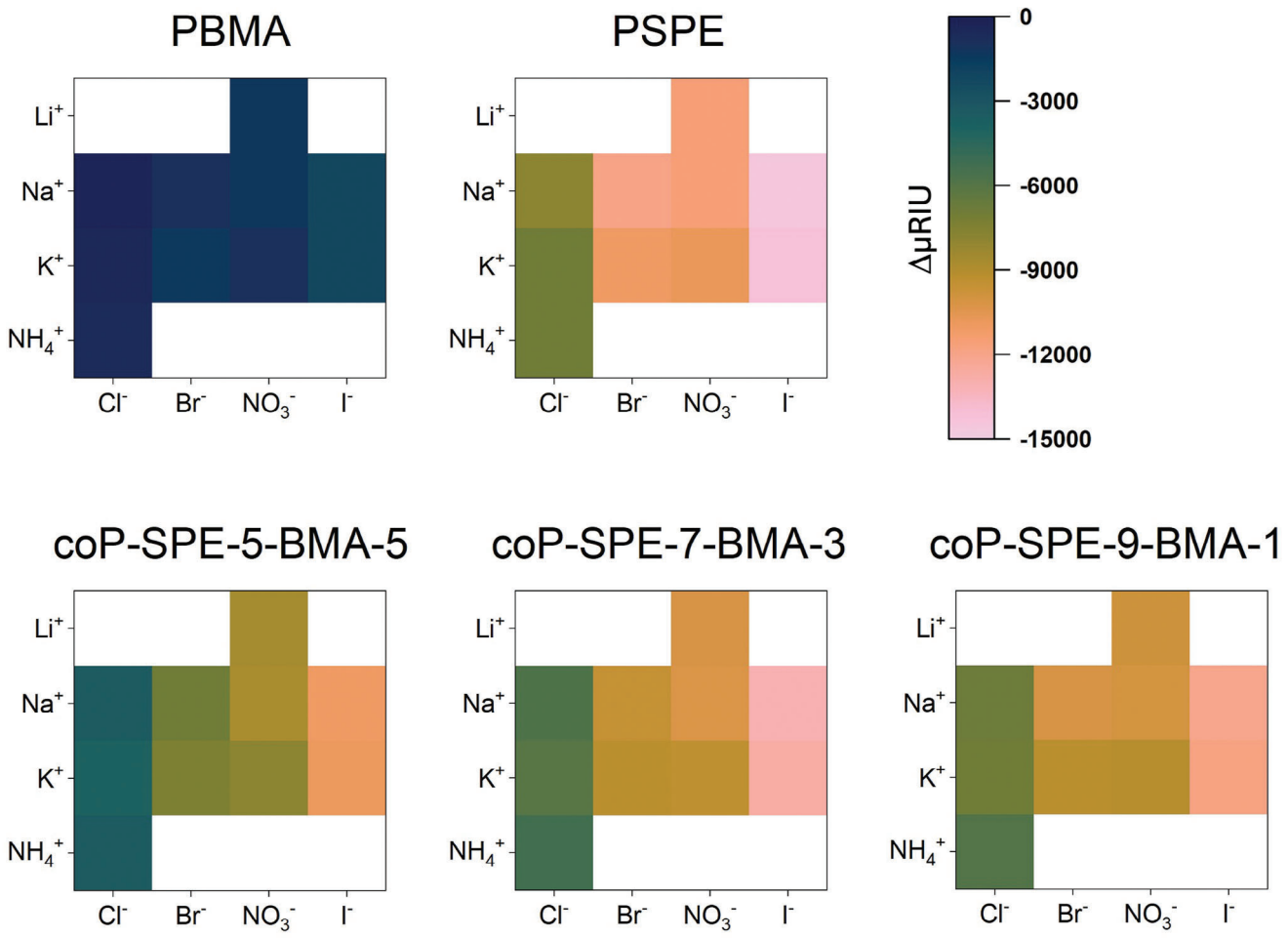

Figure 6. Comparative representation of the SPR response of amphiphilic BMA/SPE copolymer films in 150 mM solutions of different monovalent salts. The shift of the gold reference signal was subtracted in all cases to account for the different refractive indices of the electrolytes. As indicated by the colorbar in the upper right corner, blue colors reflect low SPR responses of ≈0 μRIU while pink colors indicate strongly negative SPR responses up to ≈−15000 μRIU.

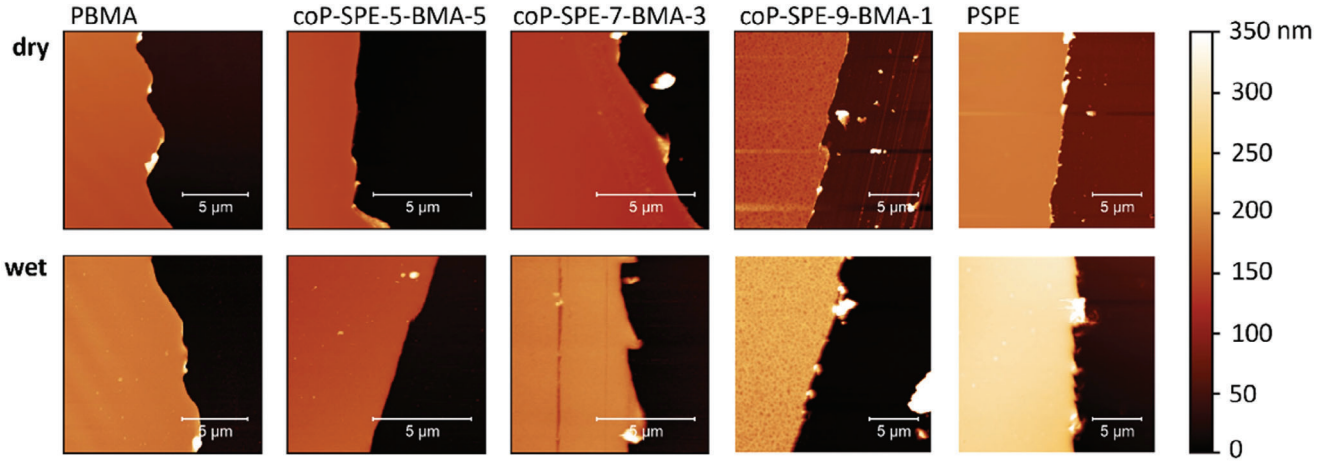

Figure 7. AFM images of the dry and wet polymers. Top: Height imaging of the film thickness at a scratch placed for measuring purposes under dry conditions. Bottom: Height imaging of the films depicted on the top immersed in Milli-Q water for 2 h.

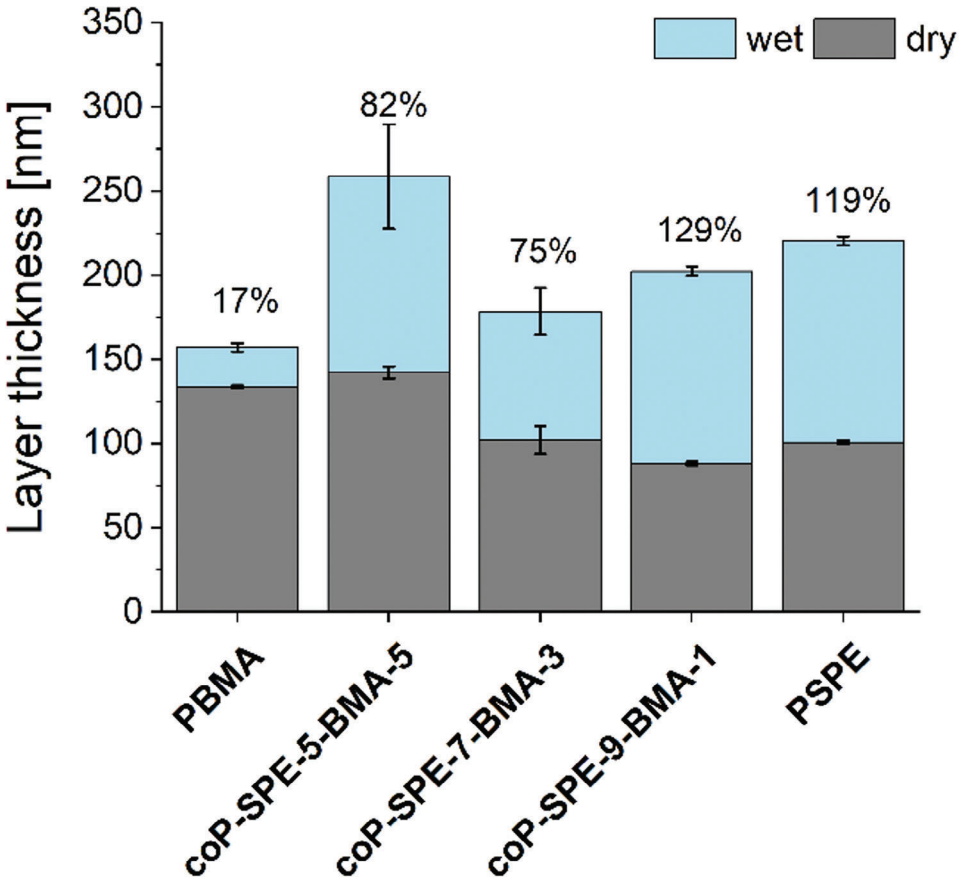

Figure 8. Thicknesses of the dry and wet polymer coating as measured by AFM. Numbers above the bars reflect the percentage increase in layer thickness after exposure to Milli-Q water. Reported values are the averages of at least 3 measurements at different positions. Error bars reflect the standard error.

3.3. Structural Analysis of the Coatings by SAXS

To gain structural insight into the morphology and internal reorganization of the polymer hydrogels at different salinities, they were coated on the inside of quartz capillaries and analyzed by SAXS. First, the polymers were investigated without any electrolyte in the capillary and measurements were done in air (for scattering curves see Figure S1, Supporting Information). Subsequently, either Milli-Q water or 150 mM NaCl solution were added into the capillaries and SAXS patterns were acquired (**Figure 9**). The scattering curve of the polymer contribution was obtained by radial integration of the scattering patterns and subtraction of the respective background measurement (capillaries with NaCl solution, Milli-Q water, or air). This approach nearly completely removed the background caused by the medium and the contribution caused by a Kapton window at ≈4 nm^{-1} in most cases. Just for **coP-SPE-5-BMA-5** and **coP-SPE-7-BMA-3**, a residual Kapton signal was detected during the measurements in air, which can be seen in the subtracted curves (Figure S1, Supporting Information). The measurements in air did not show any distinct peaks or ordered structural features in the size range accessible by SAXS. The polymer coatings seem to be very unordered and with a homogenous polymer structure.

Upon the addition of Milli-Q water, the SAXS curve of **PBMA** remained very similar to the curve in air, while all polymers containing SPE show substantial changes in the scattering curves. For the **PSPE**, **coP-SPE-9-BMA-1**, and **coP-SPE-7-BMA-3** coatings, scattering contributions at 0.1–3 nm^{-1} appeared, while **coP-SPE-5-BMA-5** showed a scattering curve intermediate between the ones of **PSPE** and **PBMA**. The Kratky plot of these curves indicated that defined nm-sized structures were formed for **coP-SPE-7-BMA-3**, **coP-SPE-9-BMA-1**, and **PSPE**, but not for **PBMA** and **coP-SPE-5-BMA-5** (inset in Figure 9A). Performing Guinier analysis and PDDF fits (from indirect Fourier transformation of the data starting from the Guinier region) on curves with obvious structures present, a radius of gyration (R_g) and maximal dimension (D_{max}) can be obtained (**Table 3**). The polymers showed an increasing R_g and D_{max} with increasing hydrophilic content (Table 3).

In 150 mM NaCl solution, all copolymers and **PSPE** showed features in the q-range between 0.1 and ≈2 nm^{-1} and the formation of a defined structure in the Kratky plot, while **PBMA** still showed a featureless scattering curve (Figure 9B). The fitted R_g from the Guinier and PDDF analysis as well as the D_{max} increased from **coP-SPE-5-BMA-5** over **coP-SPE-9-BMA-1** to **PSPE**, while **coP-SPE-7-BMA-3** had the most pronounced structural features and larger sizes. This agreed with the shift of the scattering contributions toward lower q-values in the scattering curve compared to the other polymers at this salt concentration.

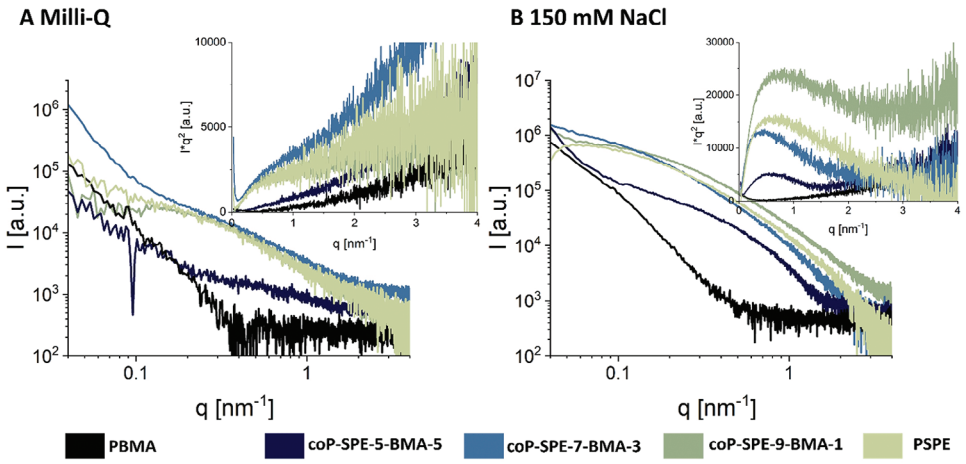

Figure 9. Scattering curves of amphiphilic polymer coatings, pure **PSPE**, and **PBMA** A) in Milli-Q water and B) in 150 mM NaCl solution. The insets show the Kratky plots.

To understand the structural response of the polymers to changes in the electrolyte, SAXS curves were acquired after adding different salt concentrations into the quartz capillaries. Due to the limited beamtime, we had to focus on the study of one polymer. **PSPE** was selected which was studied in Milli-Q water and at different NaCl concentrations of 1, 2, 5, 10, 20, 50, 100, 200, and 500 mM. At a concentration of 1000 mM, the scattering contrast started to reduce strongly, so that the scattering signal of the swollen polymer could no longer be reliably detected. As this loss of contrast occurred at high salinities, the lower salinity solutions had a lower electron density which differed enough from the polymer (also containing electron-rich sulfate moieties) to create a scattering contrast. The scattering curves (**Figure 10A**) showed an increase of the scattering intensity between 0.1 and 3 nm^{-1} with increasing NaCl concentration. An initial steep decay of the scattering curve was visible at $q<0.1$ nm^{-1} whose magnitude decreased with increasing salt concentration. This steeper slope at low q values is an indication of an agglomerated state and indicates that the polymer was not yet fully unfolded and larger agglomerates were still present. These agglomeration features can be interpreted as areas of compact, collapsed polymer at low salt concentrations. At higher salt concentrations, the polymers were more swollen so that the polymer chains were further away from each other, and no agglomeration could be observed anymore.

Table 3. Guinier R_g and PDDF fit parameters of the scattering curves of the amphiphilic copolymers and **PSPE** in Milli-Q water and 150 mM NaCl solution.

	Sample	Guinier R_g [nm]	R_g PDDF [nm]	D_{max} [nm]
Milli-Q	**coP-SPE-5-BMA-5**	6.8 ± 5.7[a)]	–	–
	coP-SPE-7-BMA-3	5.2 ± 0.4	5.5 ± 0.4	19.7 ± 1.7
	coP-SPE-9-BMA-1	7.0 ± 3.7	6.8 ± 2.7	23.3 ± 5.8
	PSPE	10.4 ± 4.3	10.2 ± 1.9	33.3 ± 3.4
150 mM	**PBMA**	8.8 ± 6.4[a)]	–	–
	coP-SPE-5-BMA-5	8.5 ± 0.9	7.4 ± 0.7	22.3 ± 2.1
	coP-SPE-7-BMA-3	12.7 ± 0.4	12.2 ± 0.5	38.7 ± 1.7
	coP-SPE-9-BMA-1	8.5 ± 0.5	8.9 ± 0.6	31.3 ± 3.8
	PSPE	10.3 ± 0.3	10.8 ± 0.3	36.3 ± 1.9

[a)] Scattering curves were dominated by the Porod decay, no unambiguous Guinier contribution could be fitted

To understand the structural response of the polymers to changes in the electrolyte, SAXS curves were acquired after adding different salt concentrations into the quartz capillaries. Due to the limited beamtime, we had to focus on the study of one polymer. **PSPE** was selected which was studied in Milli-Q water and at different NaCl concentrations of 1, 2, 5, 10, 20, 50, 100, 200, and 500 mM. At a concentration of 1000 mM, the scattering contrast started to reduce strongly, so that the scattering signal of the swollen polymer could no longer be reliably detected. As this loss of contrast occurred at high salinities, the lower salinity solutions had a lower electron density which differed enough from the polymer (also containing electron-rich sulfate moieties) to create a scattering contrast. The scattering curves (**Figure 10A**) showed an increase of the scattering intensity between 0.1 and 3 nm^{-1} with increasing NaCl concentration. An initial steep decay of the scattering curve was visible at $q<0.1$ nm^{-1} whose magnitude decreased with increasing salt concentration. This steeper slope at low q values is an indication of an agglomerated state and indicates that the polymer was not yet fully unfolded and larger agglomerates were still present. These agglomeration features can be interpreted as areas of compact, collapsed polymer at low salt concentrations. At higher salt concentrations, the polymers were more swollen so that the polymer chains were further away from each other, and no agglomeration could be observed anymore.

The Kratky plot (Figure 10B) also changed with increasing salt concentration. In Milli-Q water, the curve was reaching a plateau while with increasing salt concentration, the curves got more bell-shaped. The bell shape of the Kratky curves indicates a compact structure while plateauing curves are a sign of unstructured, random samples.[30] At low salinity, and subsequently a low degree of swelling, the polymer chains revealed a more random conformation without much space in between, while at high salinities, the polymer was swollen with separated and stretched chains, forming larger water pockets.

A closer look at the pair-distance distribution using a p(R) analysis revealed a maximum between 2 and 5 nm for all curves (Figure 10D). The curve shapes in the vicinity of the maximum showed only subtle changes with increasing salt concentration (Figure 10D). The maximum in the p(r) curves increased for increasing NaCl concentrations. This suggests that the formation of larger structures overcompensated the decrease in scattering contrast between polymer and salt solution. While the position of the maximum in the p(r) curves was barely affected by the changed NaCl concentrations, the curves showed increasing contributions at higher r values, with increasing D_{max} values with increasing salt concentrations. The increase in D_{max} is connected to the increased asymmetry of the p(r) curves created by enhanced scattering contributions for r values larger than 5 nm. While the symmetry of the curves in Milli-Q water and at low NaCl concentrations reflect a rather isotropic shape of the scattering objects, the shape of the curves at higher salt concentrations with the additional contributions at larger r values indicate an uniaxial distortion like observed for cylindrical objects.[55] Since this observation does not agree with the dimensions of the polymer chains, this change in structure indicates that the p(r) curves do not reflect the shape of the isolated polymer chains, but the shape of the electrolyte pockets within the polymer matrix.

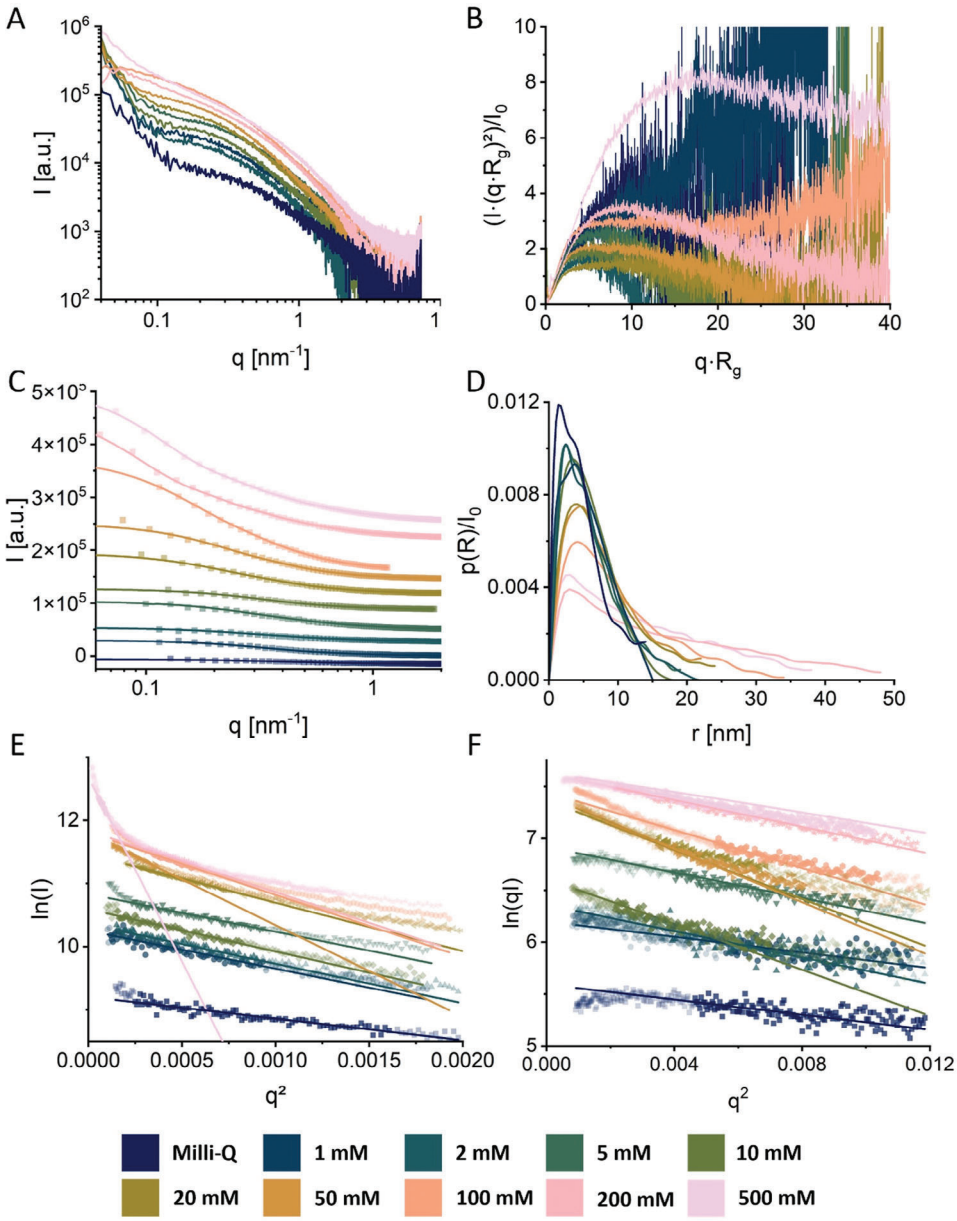

Figure 10. **A)** SAXS curves of **PSPE** films in Milli-Q water at NaCl concentrations between 1 and 500 mM NaCl. Shown are exemplary measurements after the subtraction of the respective background. **B)** Dimensionless Kratky plot. **C)** Fit of the p(R) curves. For clarity, only every 10th data point is shown, and the curves are shifted vertically. **D)** Normalized p(R) curves resulting from the fits shown in panel C. **E)** Guinier Plot with fit, data points not used for the fit are displayed in a lighter color. **F)** Cross-sectional Guinier plot with fit.

The Guinier analysis (Figure 10E) shows that in the ln(I) against q^2 plot, the upper end of the linear region shifts to lower q^2 for high salt concentrations and becomes narrower, which was connected to an increase of the length of the linear segments of the cross-sectional Guinier plot ln(qI) against q^2 (Figure 10F). This indicates larger, elongated structures for high salt concentrations independent of any shape-specific model. The obtained Porod exponents increase from 1.4 in Milli-Q water to 1.8 in 100 mM NaCl which indicate structures intermediate between stiff rods with a Porod exponent of 1 and Gaussian swollen polymer chains with a Porod exponent of 2.[47]

Based on these shape-independent results, we decided to fit the SAXS data at lower salt concentrations with a Gauss Lorentz Gel model which describes the scattering from a hydrogel structure.[48] This model fits the static correlation length, which is the distance between crosslinks or inhomogeneities in the polymer network, and the dynamic correlation length, which is a correlation length between the flexible polymer chains. The dynamic correlation length of the hydrated PSPE films increases from 1.2 nm in Milli-Q water to 2.1 nm in 50 mM NaCl, while the static correlation length increases from 5.9 nm in Milli-Q water to 7.0 nm in 50 mM NaCl (**Table 4**). This increase in distance

Table 4. Fit parameters derived from the analysis of the SAXS scattering curves of **PSPE** in Milli-Q water and 1 – 500 mM NaCl solutions. The static and dynamic correlation lengths were fitted using the Lorentz Gel model. The Porod exponent was determined using a Guinier-Porod fit, the overall D_{max} was derived from the p(R) analysis.

	Model-free (Guinier plot and GNOM indirect transform for overall structure and cross-section when appropriate)				Guinier-Porod shape-independent fit after Ref. [47]				Gauss-Lorentz gel		
Parameter	Overall R_g [nm]	Cross-sectional R_g [nm]	Overall D_{max} [nm]	Cross-sectional D_{max} [nm]	R_g [nm]	Porod exponent	Dimensionality parameter s	X^2	Corr. Length dynamic [nm]	Corr. Length static [nm]	X^2
Milli-Q	3.98 ± 0.13	–	16.3	–	3.11 ± 0.11	1.40 ± 0.0	0 ± 0.04	3.8213	1.24 ± 0.01	5.86 ± 0.22	1.2915
1 mM	4.52 ± 0.10	–	17.1	–	3.90 ± 0.15	1.41 ± 0.01	0 ± 0.04	1.155	1.46 ± 0.01	4.04 ± 0.01	1.9537
2 mM	4.86 ± 0.13	–	18.0	–	4.23 ± 0.16	1.59 ± 0.01	0 ± 0.05	1.639	1.28 ± 0.01	4.41 ± 0.09	0.9457
5 mM	4.82 ± 0.08	–	18.5	–	3.89 ± 0.09	1.62 ± 0.01	0 ± 0.03	4.0617	1.34 ± 0.01	4.83 ± 0.06	1.6727
10 mM	4.86 ± 0.08	–	18.7	–	4.27 ± 0.12	1.68 ± 0.01	0 ± 0.04	1.4527	1.54 ± 0.02	4.69 ± 0.06	1.7394
20 mM	5.41 ± 0.05	–	19.8	–	4.70 ± 0.09	1.77 ± 0.003	0 ± 0.03	3.8315	1.76 ± 0.01	4.92 ± 0.04	1.8913
50 mM	7.12 ± 0.09	1.61 ± 0.02	27.1	7.2 ± 0.5	2.32 ± 0.03	1.95 ± 0.01	0.68 ± 0.01	1.2029	2.06 ± 0.01	7.04 ± 0.07	1.6246
100 mM	7.06 ± 0.21	1.36 ± 0.02	26.9	6.7 ± 0.5	1.86 ± 0.02	1.92 ± 0.01	0.85 ± 0.07	1.2407	–	–	–
200 mM	8.89 ± 0.11	1.14 ± 0.01	31.1	4.6 ± 0.5	1.20 ± 0.01	2.23 ± 0.01	0.91 ± 0.01	1.4883	–	–	–
500 mM	15.01 ± 0.47	1.05 ± 0.01	54.4	3.9 ± 0.5	1.04 ± 0.01	2.56 ± 0.02	0.96 ± 0.01	1.5195	–	–	–

between the crosslinking points and the increase in the average distance between the flexible polymer chains is in good agreement with the screening of interactions between the zwitterionic groups occurring at high salt concentrations. As the ions in solution break the interactions between pairs of the zwitterionic moieties of the copolymers, the average distance between the polymer chains is increasing. Thus, the distance between the crosslinking points of the polymer is increasing as well, resulting in longer flexible areas of the polymer chains between the crosslinking points without the interactions between the zwitterionic side chains.

Above a concentration of 50 mM, the Gel model does not describe the measured data adequately anymore as it becomes visible from the strongly enhanced fitting discrepancy ($X^2 \gg 5$), and the system can be better described using the Guinier-Porod model for elongated, cylinder-like structures with a shape parameter s tending to 1. This uniaxial distortion of the structure becomes also obvious from the model free cross-sectional R_g and D_{max} (Table 4). Both, the crossectional R_g and crossectional D_{max}, decrease with increasing salt concentrations, while the overall D_{max} increases as also the static correlation length of the poorly fitting Gauss-Lorentz model. Taking the increases in the overall R_g and D_{max} into consideration, while the cross-sectional parameters point to thinner, elongated "tubes" forming upon an increase of ionic strength (**Figure 11**). This is in good agreement with the observed shape of the PDDF (Figure 10D) and together both analyses indicate a change in the water pore structure from compact to elongated.

A comparison between the fitted D_{max} of the SAXS curves and the SPR swelling curve (Figures 2B and 11) shows that both, the decrease in optical density due to the swelling of the polymer as observed in the SPR measurements and the increase in pore length, occur in a similar concentration range. While the change in the SPR signal provides information on the overall density and thickness changes in the polymer films, the SAXS measurements reveal the structural changes within the coatings. The extension of the pores inside the polymer film increased, while the density of the films decreased up to a NaCl concentration of 200–400 mM. Above this concentration, the maximum swelling and chain extension had been reached.

This analysis of the SAXS data leads to a model of compact water pockets within the polymer, which extend to elongated structures at higher salinities with decreasing radius in the short axis (**Figure 12**). The elongation of the water pockets is a result of the lateral constrain of the thin polymer film that hampers any unfolding of the polymer in the lateral direction. At the same time, the swelling is thermodynamically favored at high salinities due to the decreased attractive interaction between the zwitterionic groups enhancing their strong demand to form a stable hydration shell. Thus, the only direction that a swelling can occur is in the direction of the surface normal and an elongation of the

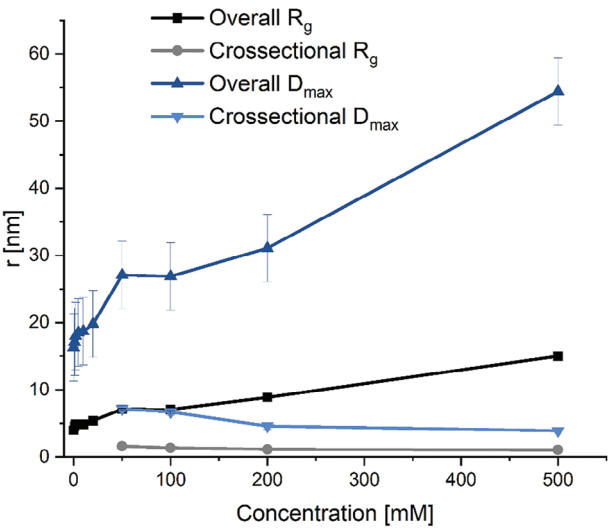

Figure 11. D_{max} and R_g of **PSPE** at different NaCl concentrations derived from Guinier analysis (R_g) and PDDF (D_{max}). Besides the model-free overall R_g and D_{max} the crossectional R_g and D_{max} are shown at higher concentrations where the fit was of a reasonable quality. The error bars are in most cases too small to be visible (compare also Table 4).

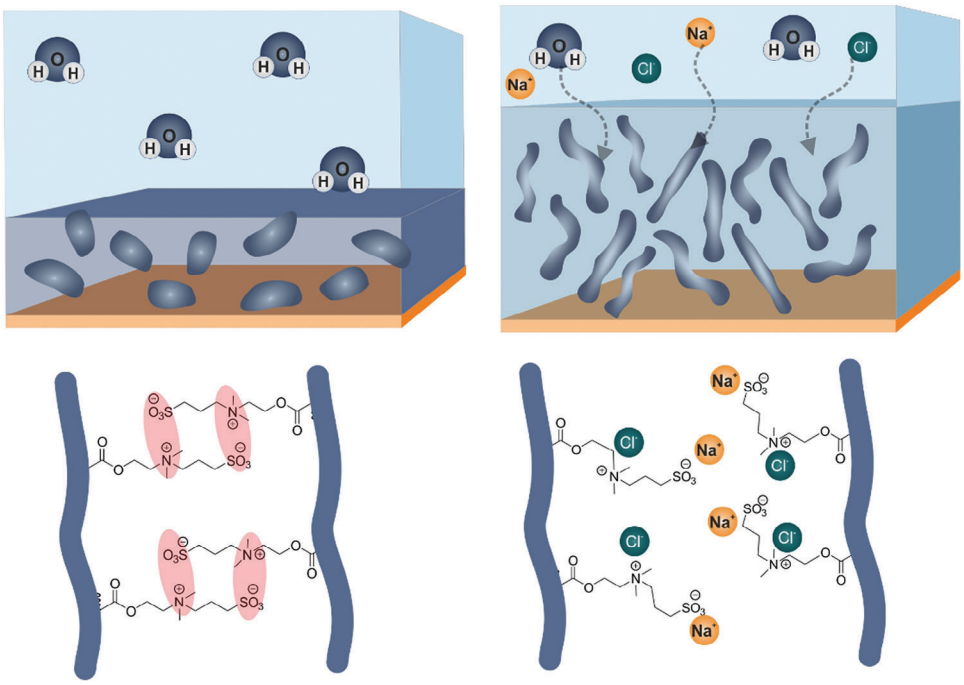

Figure 12. Schematic illustration of the swelling of **PSPE** in Milli-Q water (left) and saline solution (right).

water pockets occurs until the geometric restrictions set by the crosslinking groups in the polymer are reached. This upper limit of unfolding was determined by SPR to be at a salt concentration of ≈500 mM. It is interesting to point out that the hydration state in Milli-Q water is the isotropic state of the polymer with symmetrical water pockets, while the unfolded state at high salinities is the anisotropically distorted state.

The understanding of the antipolyelectrolyte behavior of zwitterionic polymers is highly relevant to understand their antifouling activity in high salinity media, such as sea water or physiological buffer solutions. In both cases, zwitterionic polymers show a salinity and ion dependent swelling and potentially uniaxially stretched polymer networks. The strong swelling of polymers like **PSPE** leads to a highly swollen and very soft nature, which leads to lower mechanical integrity that might facilitate small microbes such as bacteria or diatoms or suspended particles like silt to enter the hydrated network.[12] An increase of the hydrophobic content decreases the swelling and pore size in amphiphilic zwitterionic copolymers leading to a more compact structure that was found in the past to have a decreased silt uptake in seawater and better antifouling performances in field tests.[21]

4. Conclusion

The influence of the addition of hydrophobic side chains on the swelling and the structure of zwitterionic polymer coatings in different electrolytes was analyzed by a combination of SPR, AFM, and SAXS. The swelling of the polymers showed a salt concentration-dependent anti-polyelectrolyte behavior. The films responses were similar to the one of the zwitterionic homopolymer **PSPE** when the amphiphilic polymers had a content of zwitterionic SPE monomer of at least 50 mol%. The layer thickness of SPE containing copolymers approximately doubled in saline solution compared to the dry state due to a pronounced salting-in effect. A change in the hydrophilicity of the studied polymers had no substantial effect on the concentration, at which the maximum swelling was observed in SPR measurements, but only on the magnitude of the swelling. This observation was supported by the AFM measurements, which additionally revealed a smooth surface structure for all polymers except **coP-SPE-9-BMA-1**. While the studied variation of cations hardly affected the swelling behavior, the nature of the anions had a strong impact on the response of the polymers. This effect increased with their chaotropic character within the Hofmeister series. Using SAXS, the unfolding of the polymer coatings could be followed and occurred at similar salinities as in the SPR measurements. Changes in both, the polymer state and in the structure of the water pockets, were observed. While at low salinities, rather isotropic structures were found which could be described by a Gauss Lorentz gel model, the antipolyelectrolyte-effect induced a distinct uniaxial distortion of the polymer coatings along the surface normal better described by a Guinier-Porod model. With increasing hydrophobic content, decreasing size of the water pockets were observed due to the more compact nature of the coatings with stronger hydrophobic interactions. These stronger interactions were also in agreement with the AFM data which showed a lower swelling for the two highest BMA concentrations than observed for the ones with high SPE content. The used combination of SPR, AFM, and SAXS measurements have proven to be a new powerful approach to understand the swelling of polymer coatings. The method has been applied to understand the antipolyelectrolyte behavior of thin, amphiphilic zwitterionic hydrogel coatings, which is crucial to tailor their mechanical properties and swelling response for low-fouling applications in electrolyte solutions, such as the ocean or in medical environments.

Supporting Information

Supporting Information is available from the Wiley Online Library or from the author.

Acknowledgements

The authors gratefully acknowledge funding by the Deutsche Forschungsgemeinschaft (DFG) GRK2376/331085229, LA 611/14, RO 2524/4, and ONR N00014-20-12244. This work is supported by the "Center for Solvation Science ZEMOS", funded by the German Federal Ministry of Education and Research BMBF and by the Ministry of Culture and Research of Nord Rhine-Westphalia. This work benefited from the use of the SasView application, originally developed under NSF award DMR-0520547. SasView contains code developed with funding from the European Union's Horizon 2020 research and innovation programme under the SINE2020 project, grant agreement No 654000.

Conflict of Interest

The authors declare no conflict of interest.

Data Availability Statement

The data that support the findings of this study are available from the corresponding author upon reasonable request.

Keywords

atomic force microscopy, hydrogel, small angle x-ray scattering, surface plasmon resonance spectroscopy, swelling

Received: August 5, 2024
Revised: October 11, 2024
Published online: November 9, 2024

[1] Q. Shao, S. Jiang, *Adv. Mater.* **2015**, *27*, 15.
[2] C. Ventura, A. J. Guerin, O. El-Zubir, A. J. Ruiz-Sanchez, L. I. Dixon, K. J. Reynolds, M. L. Dale, J. Ferguson, A. Houlton, B. R. Horrocks, A. S. Clare, D. A. Fulton, *Biofouling* **2017**, *33*, 892.
[3] A. Laschewsky, A. Rosenhahn, *Langmuir* **2019**, *35*, 1056.
[4] Y. Higaki, M. Kobayashi, A. Takahara, *Langmuir* **2020**, *36*, 9015.
[5] C. A. Del Grosso, C. Leng, K. Zhang, H.-C. Hung, S. Jiang, Z. Chen, J. J. Wilker, *Chem. Sci.* **2020**, *11*, 10367.
[6] Z. Chen, *Langmuir* **2022**, *38*, 4483.
[7] E. Ostuni, R. G. Chapman, R. E. Holmlin, S. Takayama, G. M. Whitesides, *Langmuir* **2001**, *17*, 5605.
[8] A. Rosenhahn, S. Schilp, H. J. Kreuzer, M. Grunze, *Phys. Chem. Chem. Phys.* **2010**, *12*, 4275.
[9] C. Leng, H. C. Hung, S. Sun, D. Wang, Y. Li, S. Jiang, Z. Chen, *ACS Appl. Mater. Interfaces* **2015**, *7*, 16881.
[10] J. Koc, E. Schönemann, A. Amuthalingam, J. Clarke, J. A. Finlay, A. S. Clare, A. Laschewsky, A. Rosenhahn, *Langmuir* **2019**, *35*, 1552.
[11] E. Schönemann, A. Laschewsky, A. Rosenhahn, *Polymers (Basel)* **2018**, *10*, 639.
[12] J. Koc, T. Simovich, E. Schönemann, A. Chilkoti, H. Gardner, G. W. Swain, K. Hunsucker, A. Laschewsky, A. Rosenhahn, *Biofouling* **2019**, *35*, 454.
[13] C. C. Yang, C. T. Lo, Y. L. Luo, A. Venault, Y. Chang, *ACS Biomater. Sci. Eng.* **2021**, *7*, 1031.
[14] C. S. Gudipati, C. M. Creenlief, J. A. Johnson, P. Prayoncpan, K. L. Wooley, *J Polym Sci A Polym Chem* **2004**, *42*, 6193.
[15] S. Krishnan, N. Wang, C. K. Ober, J. A. Finlay, M. E. Callow, J. A. Callow, A. Hexemer, K. E. Sohn, E. J. Kramer, D. A. Fischer, *Biomacromolecules* **2006**, *7*, 1449.
[16] R. Quintana, D. Jańczewski, V. A. Vasantha, S. Jana, S. S. C. Lee, F. J. Parra-Velandia, S. Guo, A. Parthiban, S. L. M. Teo, G. J. Vancso, *Colloids Surf B Biointerfaces* **2014**, *120*, 118.
[17] J. H. Kardela, I. S. Millichamp, J. Ferguson, A. L. Parry, K. J. Reynolds, N. Aldred, A. S. Clare, *ACS Appl. Mater. Interfaces* **2019**, *11*, 29477.
[18] F. Koschitzki, R. Wanka, L. Sobota, J. Koc, H. Gardner, K. Z. Hunsucker, G. W. Swain, A. Rosenhahn, *ACS Appl. Mater. Interfaces* **2020**, *12*, 34148.
[19] G. Galli, E. Martinelli, *Macromol. Rapid Commun.* **2017**, *38*, 1600704.
[20] A. K. Leonardi, C. K. Ober, *Annu. Rev. Chem. Biomol. Eng.* **2019**, *10*, 241.
[21] L. Schardt, A. Martínez Guajardo, J. Koc, J. L. Clarke, J. A. Finlay, A. S. Clare, H. Gardner, G. W. Swain, K. Hunsucker, A. Laschewsky, A. Rosenhahn, *Macromol. Rapid Commun.* **2022**, *43*, 2100589.
[22] J. C. Salamone, W. Volksen, A. P. Olson, S. C. Israel, *Polymer (Guildf)* **1978**, *19*, 1157.
[23] T. Sakamaki, Y. Inutsuka, K. Igata, K. Higaki, N. L. Yamada, Y. Higaki, A. Takahara, *Langmuir* **2019**, *35*, 1583.
[24] P. Mary, D. D. Bendejacq, M.-P. Labeau, P. Dupuis, *J. Phys. Chem. B* **2007**, *111*, 7767.
[25] S. Katayama, A. Myoga, Y. Akahori, *Journal of Physical Chemistry* **1992**, *96*, 4698.
[26] M. Gao, K. Gawel, B. T. Stokke, *Eur. Polym. J.* **2014**, *53*, 65.
[27] Y. Zhou, J. Li, Y. Zhang, D. Dong, E. Zhang, F. Ji, Z. Qin, J. Yang, F. Yao, *J. Phys. Chem. B* **2017**, *121*, 800.
[28] J. De Grooth, W. Ogieglo, W. M. De Vos, M. Gironès, K. Nijmeijer, N. E. Benes, *Eur. Polym. J.* **2014**, *55*, 57.
[29] A. R. Berens, H. B. Hopfenberg, *Polymer (Guildf)* **1978**, *19*, 489.
[30] T. Xiang, T. Lu, W. F. Zhao, C. S. Zhao, *Langmuir* **2019**, *35*, 1146.
[31] S. Paschke, F. Marx, V. Bleicher, A. Eickenscheidt, K. Lienkamp, *Macromol. Chem. Phys.* **2023**, *224*, 2200334.
[32] Z. Yang, S. Zhang, V. V. Tarabara, M. L. Bruening, *Macromolecules* **2018**, *51*, 1161.
[33] C.-H. Lin, S.-C. Luo, *Langmuir* **2021**, *37*, 12476.
[34] C. Leng, X. Han, Q. Shao, Y. Zhu, Y. Li, S. Jiang, Z. Chen, *J. Phys. Chem. C* **2014**, *118*, 15840.
[35] T. Wang, X. Wang, Y. Long, G. Liu, G. Zhang, *Langmuir* **2013**, *29*, 6588.
[36] E. Schönemann, J. Koc, N. Aldred, A. S. Clare, A. Laschewsky, A. Rosenhahn, E. Wischerhoff, *Macromol. Rapid Commun.* **2020**, *41*, 1900447.
[37] I. Lokteva, M. Koof, M. Walther, G. Grübel, F. Lehmkühler, *Small* **2019**, *15*, 1900438.
[38] C. E. Blanchet, A. Spilotros, F. Schwemmer, M. A. Graewert, A. Kikhney, C. M. Jeffries, D. Franke, D. Mark, R. Zengerle, F. Cipriani, S. Fiedler, M. Roessle, D. I. Svergun, *J. Appl. Crystallogr.* **2015**, *48*, 431.
[39] D. Franke, A. G. Kikhney, D. I. Svergun, *Nucl Instrum Methods Phys Res A* **2012**, *689*, 52.
[40] P. V. Konarev, V. V. Volkov, A. V. Sokolova, M. H. J. Koch, D. I. Svergun, *J. Appl. Crystallogr.* **2003**, *36*, 1277.
[41] K. Manalastas-Cantos, P. V. Konarev, N. R. Hajizadeh, A. G. Kikhney, M. V. Petoukhov, D. S. Molodenskiy, A. Panjkovich, H. D. T. Mertens, A. Gruzinov, C. Borges, C. M. Jeffries, D. I. Svergun, D. Franke, *J. Appl. Crystallogr.* **2021**, *54*, 343.
[42] D. I. Svergun, *J. Appl. Crystallogr.* **1992**, *25*, 495.
[43] M. Doucet, J. H. Cho, G. Alina, Z. Attala, J. Bakker, W. Bouwman, P. Butler, K. Campbell, T. Cooper-Benun, C. Durniak, L. Forster, M. Gonzalez, R. Heenan, A. Jackson, S. King, P. Kienzle, J. Krzywon, R. Murphy, T. Nielsen, L. O'Driscoll, W. Potrzebowski, S. Prescott, R.

Ferraz Leal, P. Rozyczko, T. Snow, A. Washington, **2021**, https://doi.org/10.5281/zenodo.3930097.
[44] A. Guinier, G. Fournet, *Small-Angle Scattering of X-Rays*, John Wiley & Sons, New York **1955**.
[45] D. I. Svergun, L. A. Feiğin, G. W. Taylor, *Structure analysis by small-angle x-ray and neutron scattering* (Ed.: G. W. Taylor), Plenum Press, New York **1987**.
[46] O. Glatter, *Scattering Methods and their Application in Colloid and Interface Science*, 1st ed., Elsevier, Amsterdam, The Netherlands, **2018**.
[47] B. Hammouda, *J. Appl. Crystallogr.* **2010**, *43*, 716.
[48] G. Evmenenko, E. Theunissen, K. Mortensen, H. Reynaers, *Polymer* **2001**, *42*, 2907.
[49] J. B. Schlenoff, *Langmuir* **2014**, *30*, 9625.
[50] J. D. Delgado, J. B. Schlenoff, *Macromolecules* **2017**, *50*, 4454.
[51] S. Z. Moghaddam, E. Thormann, *J. Colloid Interface Sci.* **2019**, *555*, 615.
[52] H. I. Okur, J. Hladílková, K. B. Rembert, Y. Cho, J. Heyda, J. Dzubiella, P. S. Cremer, P. Jungwirth, *J. Phys. Chem. B* **2017**, *121*, 1997.
[53] P. Lo Nostro, B. W. Ninham, *Chem. Rev.* **2012**, *112*, 2286.
[54] Y. Zhang, P. S. Cremer, *Annu. Rev. Phys. Chem.* **2010**, *61*, 63.
[55] D. I. Svergun, M. H. J. Koch, *Rep. Prog. Phys.* **2003**, *66*, 1735.